

SHUNTS IN SILICON SOLAR CELLS BELOW SCREEN PRINTED SILVER CONTACTS

F. Huster¹, S. Seren¹, G. Schubert¹, M. Kaes¹, G. Hahn¹, O. Breitenstein²¹University of Konstanz, Department of Physics, P.O.Box X916, D-78457 Konstanz, Germany²Max Planck Institute of Microstructure Physics, Weinberg 2, D-06120 Halle, GermanyAuthor for correspondence: Frank.Huster@uni-konstanz.de, Tel.: +49-7531 88 4469, Fax: +49-7531 88 3895

ABSTRACT: Shunts below fired contacts of a fritted Ag paste were investigated using lock-in thermography and IV-measurements. Experiments were carried out on single point contacts to p-type silicon and on solar cells with process induced and intentionally introduced shunts. All shunts below contacts exhibited a combination of ohmic and rectifying behavior. The IV characteristics of the point contacts were excellently modeled using an equivalent circuit comprising a diode, a low parallel shunt resistance and a limiting spreading resistance due to the small contact size. For shunted solar cells the double diode model is extended by adding this shunt equivalent circuit. As a main cause for cell degradation upon over-firing an increase in contact resistance was identified, while no severe shunts below contacts were observed. A model to explain the occurrence of a rectifying and an ohmic contact of Ag to lowly doped silicon is proposed.

Keywords: Shunts - 1, Contact - 2, c-Si - 3

1 INTRODUCTION

Crystalline silicon solar cells, produced in an industrial environment and equipped with screen printed contacts, generally have only moderate shunt resistances between 1000 and 5000 Ωcm^2 and show often some deviation of the IV curve from the ideal double diode model. Both observations are assumed to be connected to process induced ohmic and rectifying shunts. In this work we investigated shunts located below fired silver thick film contacts with the purpose of building a microscopic picture and determining the origin of the shunt.

Despite the importance of avoiding or controlling process induced shunts, little is known about the origin and the physics of shunt contacts below fired thick-film contacts. Shunts in metallized cell areas are (mostly) direct contacts of the front contact to the p-type base. There are two main ways of shunt formation: mechanical damage of the emitter before or during metallization and etching of the fritted silver paste through the emitter during contact firing, on extended areas or localised at small spikes. Shunts formed by the first way demand for a more careful wafer handling, those formed by the second show the need for a better process control and further paste development.

The interface of a fired metal paste contact of a silicon solar cell is, in terms of chemical composition and geometry, highly undefined. It might behave quite differently from the intensively investigated metal-semiconductor contacts normally used for semiconductor devices other than industrial solar cells. Therefore, we started our investigations by measuring the IV characteristics of printed and fired Ag-contacts on p-type silicon. A second experiment dealt with shunts in standard processed solar cells. Are the shunts mostly below grid lines? Do they exhibit an ohmic or a rectifying characteristic? Are they correlated to emitter damage before metallisation? In a third experiment the emitter was intentionally damaged before metallization. In a fourth and final experiment the effect of over-firing was investigated. The shunt detection and characterisation was done using conventional lock-in thermography [1] with external voltage modulation (in the following referenced as VomLIT), the recently introduced light modulated lock-in thermography [2] (LimoLIT) and IV measurements with a fitting to a triple diode model.

2 SINGLE AG POINT CONTACTS ON P-TYPE SI

2.1 Measurements

Several point contacts of a commercial screen printing silver paste (containing glass frit for etching through SiN_x) were prepared and the IV-curves measured with a 4-point-probe setup. Details of the samples are given in Tables I and II. The firing was done in a belt furnace with firing conditions close to standard firing.

A typical example of the IV curve is shown in Fig. 1. For voltages larger than ± 1 V some deviations from the equivalent circuit modeling occurred, probably due to Schottky barrier lowering effects and maybe contact heating. The measurements showed good reproducibility.

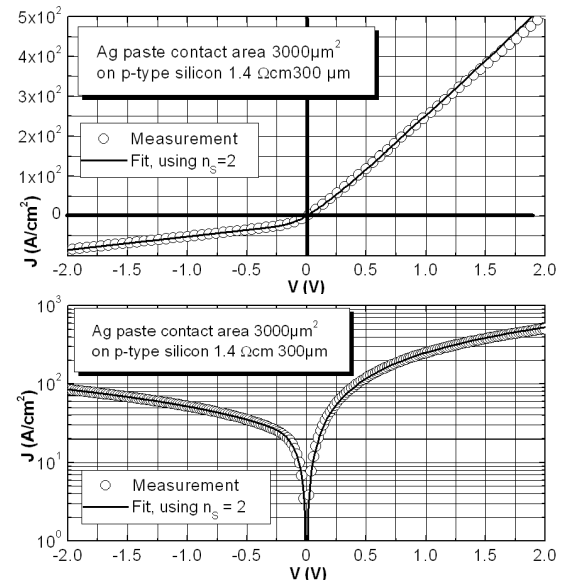


Figure 1: Typical IV-measurement of a single point contact (point A5 in Table I) on a linear and a log scale.

From the IV characteristic a diode i.e. rectifying behaviour is obvious, but also a significant reverse current. Note the large current densities, which might be well over 10^3 A/cm^2 if only a small fraction of the contact area actually contributes to the current transport¹.

¹ An area fraction of 0.01 to 10% is suggested by recent investigations on the microstructure of Ag paste emitter contacts.

2.2 Theory [3] and modeling

For an ideal contact of silver to lowly doped p-type silicon ($N_A \approx 10^{16} \text{ cm}^{-3}$) a rectifying IV characteristic is predicted with a saturation current $J_{S,0} = 0.002 \text{ A/cm}^2$ independent of doping concentration, a $J_{S,0}$ temperature dependence of $\approx 0.7\%/K$ and an ideality factor n close to 1 ($T = 298 \text{ K}$). The spreading resistance R_{SR} of a circular contact of radius r on a substrate with resistivity ρ and thickness W can be approximately calculated as:

$$R_{SR} = \frac{\rho}{2\pi \cdot r} \arctan\left(\frac{2W}{r}\right) \approx \frac{\rho}{4 \cdot r} \quad (\text{for } W \gg r)$$

The IV-curves of all contacts can be excellently modelled using a simple equivalent circuit shown in Fig. 2.

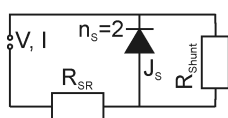


Figure 2: Equivalent circuit of a fired silver point contact to p-type silicon. R_{SR} is the spreading resistance in the lowly doped silicon wafer.

2.3 Fitting results

A remarkable consistency of the calculated spreading resistance and the fitted series resistance is apparent. The very low shunt resistance (of the order of normal emitter contact resistance!) as well as the high saturation current are not explained by the simple theory of the ideal Schottky diode. A Schottky diode ideality factor $n_s \approx 2$ was a good choice for all measurements, but with a possible range between 1.5 and 2.5.

Table I: Point contacts of fritted silver paste on p-type mc silicon, $1.4 \text{ } \Omega\text{cm}$, thickness $300 \text{ } \mu\text{m}$, 75 nm PECVD- SiN_x on top. Back side contact: full area screen printed aluminium. The Schottky diode is modelled with $n_s=2$.

Point	Contact area	Calculated spreading resistance	Fit using equiv. circ. Fig. 2		
			Series resist.	Shunt resist.	$J_{S,0}$
	μm^2	Ω	Ω	Ωcm^2	A/cm^2
A1	7900	66	59	0.0300	16.5
A2	10300	57	55	0.0216	22.3
A3	7900	66	61	0.0284	20.3
A4	3800	97	98	0.0255	21.1
A5	3000	110	118	0.0264	20.7
Avg.	-	-	-	0.026	20.6

Table II: Same configuration as described in Tab. I, but on a different substrate: bare silicon, polished p-type (100)-FZ, $0.6 \text{ } \Omega\text{cm}$, thickness $260 \text{ } \mu\text{m}$.

Point	Contact area	Calculated spreading resistance	Fit using equiv. circ. Fig. 2		
			Series resist.	Shunt resist.	$J_{S,0}$
	μm^2	Ω	Ω	Ωcm^2	A/cm^2
B1	28400	13	12.5	0.0139	22.9
B2	12600	21	18	0.0111	30.2
Avg.	-	-	-	0.013	26.5

3 SHUNTS IN CZ CELLS: STANDARD PROCESS

A set of 10 Cz wafers was processed in a standard industrial process (NaOH etch, POCl_3 diffusion $50 \text{ } \Omega/\text{sq}$, P-glass removal, PECVD- SiN_x , screen printing and firing, edge isolation with dicing saw). Many shunts are clearly visible in LimoLIT (Fig. 3 and 4) as well as in VomoLIT thermograms (Fig. 5), almost all below contacts. The emitter scratch on the representative wafer shown in this section (outstanding shunt in the pictures in the upper right corner) is discussed in section 4.

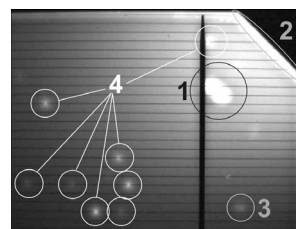


Figure 3: Zoom into the right LimoLIT thermogram of Fig. 4. “1” denotes the emitter scratch shunt; “2” (open p/n-junction after edge isolation) and “3” are examples of recombinaive shunts not correlated to the metallization. “4” is assigned to shunts below contacts.

Using the LimoLIT measurement technique it is possible to look for any emitter damage before metallization, usually being visible as a recombinaive shunt. Only small recombination activities (besides recombination at damaged wafer edges) are observable in Fig. 4 on the left, which are obviously not correlated to the shunts found after metallization, see Fig. 4 right picture. From this we conclude that the shunts in these cells are not caused by a locally missing emitter.

In Fig. 5 the voltage symmetry of the shunts is checked by VomoLIT in reverse and forward bias. Most of the shunts appear to be predominantly ohmic.

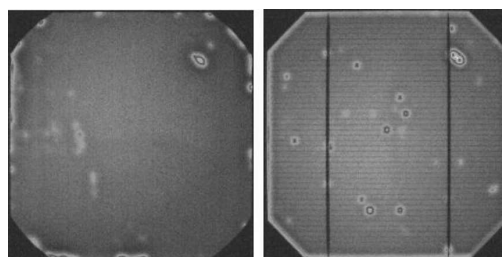


Figure 4: LimoLIT measurements of a Cz-Si cell: before metallization (left) and finished cell after metallization and edge isolation (right). Many shunts below grid lines are visible in the right picture, which are apparently not correlated to any surface damage before metallization (except scratch).

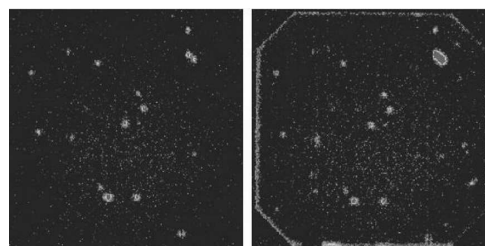


Figure 5: Same cell as in Fig.4/right, investigated by VomoLIT without illumination in reverse (left) and forward (right) bias of $\pm 0.5 \text{ V}$. The edge recombination and the scratch are (partly) rectifying shunts, whereas most of the other shunts seem to be ohmic. This was observed for the whole set of investigated cells.

4 SOLAR CELLS WITH INTENTIONALLY DAMAGED EMITTERS

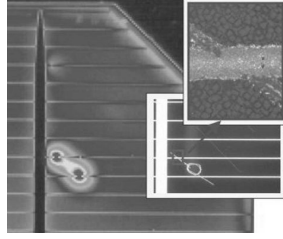
By intentionally damaging the emitter before metallization shunts can be generated that are, to some extent, well defined as point contacts comparable to section 2. This was done using a diamond scribe (see. Fig. 6) and

a dicing saw (Fig. 8 and 9). The concomitantly induced shunts in the damaged p/n-junction beneath the metal to groove cross-points play a minor role. In subsection 4.1 the voltage dependence of a single shunt is investigated, while in 4.2 cells with a large number of shunts are characterized.

4.1 Emitter is damaged by a diamond scriber

The voltage characteristic of a shunt (in the sense of being ohmic and/or rectifying) can be extracted from contacted thermography by measuring with a bias voltage scan. The emitter scratch mentioned in section 3 and displayed in Fig. 6 was investigated that way.

Figure 6: Detail of the LimoLIT thermogram in Fig. 4, in the region of the diamond scriber scratch. The insets show optical microscope pictures of the scratch and a cross-point.



In the voltage scan depicted in Fig. 7 two regions of linear voltage dependence can be seen. Due to our differential lock-in measuring technique using small bias modulation (0.1 V) the temperature modulation signal in the shunt area is proportional to $\text{abs}(V_{\text{bias}}/R)$. According to the equivalent circuit in Fig. 2 the resistance in reverse bias is determined by the series connection of R_{SR} and R_{Shunt} , while in forward bias R_{Shunt} is short-circuited by the fully opened Schottky diode (at least above 0.2 V).

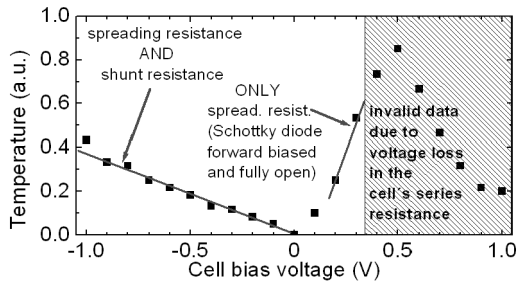


Figure 7: Voltage modulated thermography: signal amplitude (temperature) averaged over a small area around the scratch shown in Fig. 6 and scanned for a range of bias voltage. Above a bias voltage ≈ 0.4 V the increasing voltage drop along the cell series resistance leads to a decrease of the actual shunt (bias) voltage.

4.2 Emitter is damaged by grinding grooves

Another set of Cz cells received emitter damage by grinding shallow grooves into the SiN_x and the emitter before metallization. The dark IV curves were fitted using the triple diode model explained in Fig. 10.

Figure 8: Optical microscope picture of a cross-point of the 150 μm wide screen printed finger and the 30 μm wide groove. The contact area is $\approx 20000 \mu\text{m}^2$; the precise calculation of R_{SR} is difficult due to the contact geometry.

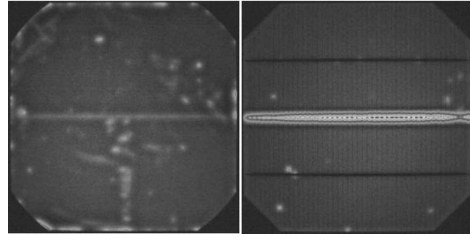
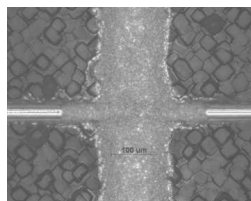


Figure 9: LimoLIT measurements of a Cz wafer with one groove cut into the emitter after SiN_x -deposition (horizontal line). Before metallization (left picture) only moderate recombination currents can be observed, whereas after metallization high shunt currents at the cross-points with the fingers are dominating.

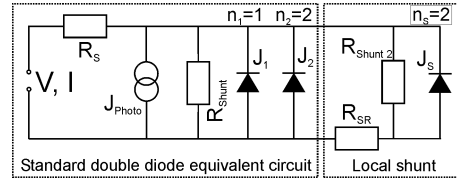


Figure 10: Equivalent circuit of a “triple diode model” to include rectifying shunts. The Schottky contact is modelled in the same manner as in Fig. 2, comprising a diode and an ohmic shunt 2 in parallel. For small, point-like Schottky contacts the shunt current is limited by a spreading resistance R_{SR} , in contrast to R_{shunt} of the double diode model. Similar models have been used before to explain humps in IV characteristics caused by junction shortage [4] or edge recombination [5].

Table III: IV parameters and parameters fitted using the equiv. circuit of Fig. 10. For comparison with the results of section 2, the fitted parameters are calculated per cross-point and cross-point area, estimated to $20000 \mu\text{m}^2$.

No. of grooves (47 cross-points per groove)	IV measurement				Fit of DARK IV $n_s=2$		
	FF %	J_{SC} mA/cm ²	V_{OC} mV	η %	R_{SR} Ω	$R_{\text{sh},2}$ Ωcm^2	$J_{\text{S},0}$ A/cm ²
0	78.8	32.9	622	16.1	-	-	-
0/scratch	78.3	32.9	622	16.1	-	-	-
1, Fig.9	73.9	32.7	619	15.0	66	0.064	2.3
2	70.9	32.8	619	14.4	82	0.072	2.1
3	69.1	32.9	619	14.1	91	0.110	0.92
4	66.7	32.9	617	13.5	98	0.126	0.88
10	55.2	32.7	601	10.8	118	0.183	0.53
Avg.	-	-	-	-	91	0.111	1.3
Calculated spreading resistance $\rho_{\text{bulk}}=1.4 \Omega\text{cm}$, thickness 300 μm :					40	-	-
For comp.: single contact Tab. II:					-	0.013	26

The diamond scratch seems to have no measurable effect on the cell parameters. Even the severe damage by a groove running across the wafer surface with 47 direct contacts of the front grid to the base is only weakening but not “killing” the cell performance. The triple diode model of Fig. 10 describes very well the experimental IV characteristics. The large differences in $R_{\text{shunt},2}$ and $J_{\text{S},0}$ compared to the single point contacts in section 2 are not understood so far. It is important to clarify if this inconsistency stems from the simplicity of the simulation model or slightly different conditions of contact preparations (firing conditions, surface/interface defects etc.).

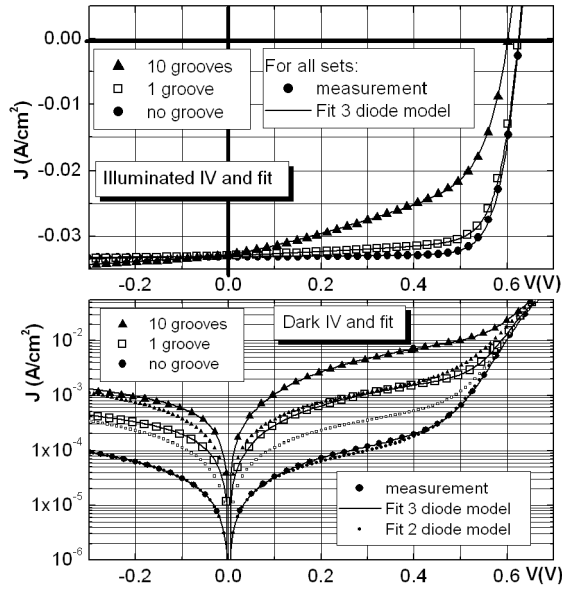


Figure 11: IV characteristics and fit curves of 3 cells with differing number of grooves. In the lower graph also the double diode fit is shown. Note the presence of a small hump (i.e. the deviation from the double diode model in the range of moderate forward voltage) even for the reference cell without grooves.

5 OVER-FIRED CELL

A strong over-firing of a screen printed cell is commonly accompanied by a severe efficiency reduction mainly caused by a degradation of the front contact. In this section the effect of a second firing (with 50% belt speed) is investigated. Surprisingly neither the number nor the strength of the shunts present after standard firing are significantly increased by the over-firing. If this is the case in general, which has to be verified with a large number of cells, lateral heat variations during contact firing could be excluded as a reason for shunts below contacts.

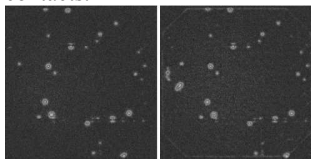


Figure 12a: Thermogram of a metallized cell after standard firing. Left: reverse biased -0.5 V, right: forward biased +0.5 V.

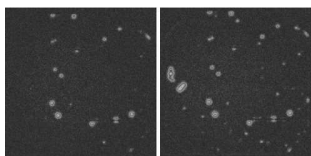


Figure 12b: Same cell, after over-firing: no significant increase or change in shunt distribution.

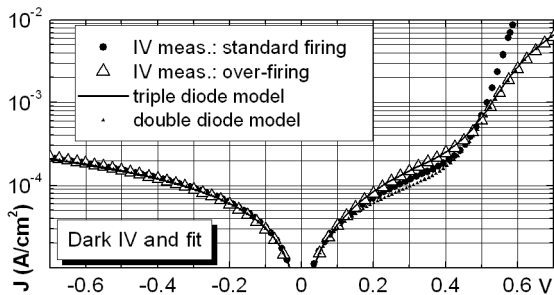


Figure 13: Dark IV measurements and fit curves of a solar cell after standard process and the same cell after a second firing with 50% belt speed (= over-firing).

Table IV: Over-fired cell: parameters and triple diode fit to dark IV curve. The main change upon second firing is the series resistance increase from 9 to 600 mΩcm², a minor change (in the sense of efficiency degradation) can be seen in the shunt spreading resistance.

Firing	FF %	J _{sc} mA/cm ²	V _{oc} mV	R _S Ω cm ²	R _{sh} Ω cm ²	Schottky diode n=2		
						J _{S,0} A/cm ²	R _{SR} Ω cm ²	R _{Sh,2} Ω cm ²
1 st	78.1	32.6	617	0.5	3200	1.5E-6	5000	6500
2 nd	28	24.5	602 T=28°	21	3300	9E-7	970	8500

6 MODEL

The shape of Ag crystallites on (100) silicon (see Fig. 14) suggests the occurrence of high electric fields at the tip of the pyramid. This field amplification can lead to a substantial barrier decrease, a well known problem of planar metal-semiconductor contacts (edge effect). Andrews [6] observed and successfully simulated a “soft” reverse breakthrough of an alloyed gold to silicon contact, assuming tip radii of the Au spikes of r ≈ 0.03 μm.

In fired Ag contacts sharp edges of Ag crystallites reaching the p-type base (either due to the size of the crystallite or due to a locally missing emitter) might exhibit an ohmic behavior caused by this electric field enhancement. At the flanks of the Ag crystallite a rectifying characteristic is plausible.

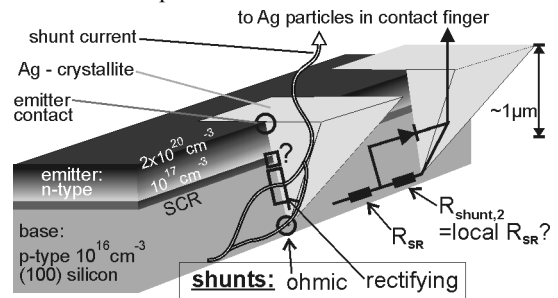


Figure 14: Model to explain the occurrence of rectifying AND ohmic shunts below fired contact fingers.

7 CONCLUSIONS

All results show that the character of shunts below fired contacts is a combination of a rectifying and an ohmic behavior. The ohmic behavior exhibits a remarkably low contact resistance for Ag on lowly doped Si, possibly explained by field enhancement at the Ag crystallite tip. Over-firing causes an increase in contact resistance but no severe shunting.

8 ACKNOWLEDGEMENTS

This work was supported by the EC within the EC2C project under contract number ENK6-CT-2001-00560.

9 REFERENCES

- [1] O. Breitenstein and M. Langenkamp, *Lock-In Thermography*, Springer 2003
- [2] M. Kaes et al., submitted to this conference
- [3] Standard text books, like S.M. Sze, *Physics of Semiconductor Devices* and E.H. Roderick, *Metal-Semiconductor Contacts*
- [4] J.E. Cotter et al., Proc. 16th EC PVSEC (2000) 1687
- [5] K.R. McIntosh et al. Proc. 16th EC PVSEC(2000) 1651
- [6] J.M. Andrews, J.Vac.Sci.Techn. vol.11/6 (1974) 972